Qin Xu[1]*, Li Wei[2] and Kang Nai[2]

[1]NOAA/National Severe Storms Laboratory, Norman, Oklahoma
[2]Cooperative Institute for Mesoscale Meteorological Studies, University of Oklahoma

1. Introduction

A three-dimensional variational (3DVar) data assimilation system was developed by Gao et al. (2013) for analyzing storm winds from radar observations. This 3DVar system can identify storm-scale mid-level vortices, but the vortex winds may not be fully resolved due to the isotropic background error covariance used for each velocity component in the cost-function. To improve the vortex winds, a two-dimensional variational (2DVar) method was developed by formulating the background error covariance with desired vortex-flow dependences in a moving frame following the mesocyclone on each tilt of radar scan (Xu et al. 2015a). This 2DVar can be extended to analyze vortex winds in a three-dimensional (3D) or even four-dimensional (4D) space. To achieve this, the vortex center location of the detected mesocyclone needs to be estimated first as a continuous function of height and time in the 4D space. After this, the analysis domain needs to be transformed into a slantwise cylindrical coordinate system moving and co-centered with the estimated vortex center in the 4D space. Then, the background error covariance functions can be formulated in the transformed coordinate system to obtain the desired vortex-flow dependences for analyzing the 3D vortex winds in the 4D space. The methodologies and related formulations developed for such an extension are presented in this paper. The effectiveness and performances of the extended method are illustrated by the results obtained for the tornadic mesocyclone that struck Moore in Oklahoma on 20 May 2013.

2. Estimating vortex center location

When a mesocyclone is detected as a by-product of the velocity dealiasing (Xu et al. 2013), its vortex center location is also estimated on each tilt of radar scan. After this estimate is fine-tuned by the two-step algorithm in section 4 of Xu et al. (2015b), the vortex center location and movement can be estimated as continuous functions of (z, t) by fitting a smooth-function form of $\mathbf{x}_c(z, t)$ constructed by B-spline basis functions to the fine-tuned vortex center locations, where $\mathbf{x}_c \equiv (x_c, y_c)$ denotes the vortex center location in the horizontal. In particular, as shown in Xu et al. (2015b), the fitting minimizes the following cost functions:

$$J(a_{kn\beta}) = \sum_i [x_c(z_i, t_i \mid a_{kn\beta}) - x_{ci}]^2,$$
$$J(b_{kn\beta}) = \sum_i [y_c(z_i, t_i \mid b_{kn\beta}) - y_{ci}]^2,$$

where $\sum_j$ denotes the summation over i, $x_c(z_i, t_i \mid a_{kn\beta}) = \sum_{kn\beta} a_{kn\beta} B_k(z_j) B_n^{\beta}(t_j)$, $y_c(z_i, t_i \mid b_{kn\beta}) = \sum_{kn\beta} b_{kn\beta} B_k(z_j) B_n^{\beta}(t_j)$, $\sum_{kn\beta}$ denotes the summation over k, n and β, $B_k(z)$ denotes the linear basis function at the k^{th} node point in z, $B_n^{\beta}(t)$ denotes the quadratic basis function of β^{th} order (with β = 0, 1) at the n^{th} node point in t, and $\mathbf{x}_{ci} = (x_{ci}, y_{ci})$ denotes the i^{th} vortex center location estimated and fine-tuned at (z_i, t_i).

For the 20 May 2013 Oklahoma Moore tornadic mesocyclone, $\mathbf{x}_c(z, t)$ is estimated by using 10 volume radial-velocity scans from the operational KTLX radar and 22 sector radial-velocity scans from the NSSL phased-array radar over the local time period from 14:52 to 15:35. The estimated $\mathbf{x}_c(z, t)$ is plotted in Fig. 1. As shown in Fig. 1, the vortex core became increasingly vertical as the mesocyclone moved toward Moore and became nearly vertical around the local time 15:13. The mesocyclone also became increasingly intense as its vortex core became increasingly vertical.

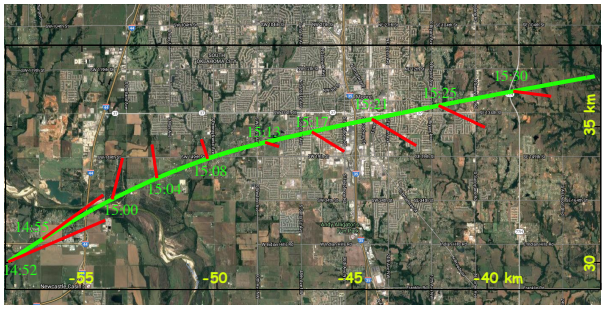

Fig. 1. Vortex center track at surface level (z = 0) plotted by green curve with local times marked in green. The red line at each marked local time shows the vertical profile of the estimated vortex center location for the height increased from z = 0 to 5 km at the fixed time. The (x, y) coordinates (labeled in yellow) are centered nearby the KTLX radar site (outside the map).

3. Coordinate transformation and flow partition

In order to formulate the background wind error correction functions in a slantwise cylindrical coordinate system co-centered with the estimated $\mathbf{x}_c(z, t)$ in the 4D space, we need to transform the local Cartesian coordinate system (x, y, z, t) first into the following coordinate system:

$$(x', y', z', t') = (x - x_c(z, t)\ ,\ y - y_c(z, t), z, t). \qquad (3.1)$$

This transformation ensures that the origin of (x', y') is co-centered and moves with $\mathbf{x}_c(z, t)$ at every vertical level. The space and time differential operators are transformed by $(\partial_x, \partial_y, \partial_z, \partial_t) = (\partial_{x'}, \partial_{y'}, \partial_{z'} - \mathbf{x}_{cz}\bullet\nabla', \partial_{t'} - \mathbf{u}_c\bullet\nabla')$, where $\mathbf{x}_{cz} = \partial_z \mathbf{x}_c$ (that is, $x_{cz} = \partial_z x_c$ and $y_{cz} = \partial_z y_c$), $\mathbf{u}_c = \mathbf{x}_{ct} = \partial_t \mathbf{x}_c$ (that is, $u_c = x_{ct} = \partial_t x_c$ and $u_c = y_{ct} = \partial_t y_c$) and $\nabla' \equiv (\partial_{x'}, \partial_{y'})$. In the transformed coordinates, the mass continuity equation can be written into

$$\nabla'\bullet(\rho_o \mathbf{u}_v) + \partial_{z'}(\rho_o w) = 0, \qquad (3.2)$$

*Corresponding author address: Qin Xu, National Severe Storms Laboratory, 120 David L. Boren Blvd., Norman, OK 73072-7326; E-mail: Qin.Xu@noaa.gov

where $\mathbf{u}_v \equiv \mathbf{u} - \mathbf{u}_c - w\mathbf{x}_{cz}$ is the horizontal component of the vortex wind in the (x', y', z', t')-coordinates, $\mathbf{u}$ is the total horizontal velocity, w is the vertical velocity, and ρ_o is the air density. Here, $\mathbf{u}_v$ is the vortex part of $\mathbf{u}$ and it can be partitioned into $\mathbf{u}_v = \mathbf{u}_s + \mathbf{u}_a$ where $\mathbf{u}_s$ (or $\mathbf{u}_a$) is the axisymmetric (or asymmetric) part of $\mathbf{u}_v$. The three-dimensional counterpart of $\mathbf{u}_v$ in (x', y', z', t') is $(\mathbf{u}_v, w) \equiv \mathbf{u}_v + w\mathbf{k}$' where $\mathbf{k}$' is the unit vector along the z'-coordinate. The three-dimensional incremental wind with respect to $\mathbf{u}_c$ in (x, y, z, t) is $\mathbf{u}_v + w\mathbf{x}_{cz} + w\mathbf{k}$ where $\mathbf{k}$ is the unit vector along the z-coordinate. This incremental wind can be also partitioned into two parts: the axisymmetric part denoted by $\mathbf{u}_s + w_s\mathbf{x}_{cz} + w_s\mathbf{k}$, and the remaining asymmetric part denoted by $\mathbf{u}_a + w_a\mathbf{x}_{cz} + w_a\mathbf{k}$.

The goal is to estimate $(\mathbf{u}_v, w)$ by fitting $\mathbf{r}_o\bullet(\mathbf{u}_v + w\mathbf{x}_{cz} + w\mathbf{k})$ to the radial-velocity innovations defined by

$$v_r^{\,i} \equiv v_r^{\,o} - w_T\sin\theta - \mathbf{r}_o\bullet\mathbf{u}_c, \tag{3.3}$$

where $v_r^{\,o}$ denotes the radar observed radial velocity, w_T (< 0) is the terminal velocity of hydrometeors, θ is the slope angle of radar beam relative to the Earth surface beneath the observation point, and $\mathbf{r}_o$ is the unit vector in the radar beam direction.

To achieve the above goal, we need to estimate $(\mathbf{u}_s, w_s)$ in the first step by fitting $\mathbf{r}_o\bullet(\mathbf{u}_s + w_s\mathbf{x}_{cz} + w_s\mathbf{k})$ to $v_r^{\,i}$, and then estimate $(\mathbf{u}_a, w_a)$ in the second step by fitting $\mathbf{r}_o\bullet(\mathbf{u}_a + w_a\mathbf{x}_{cz} + w_a\mathbf{k})$ to the updated radial-velocity innovations defined by

$$v_r^{\,is} \equiv v_r^{\,i} - \mathbf{r}_o\bullet(\mathbf{u}_s + w_s\mathbf{x}_{cz} + w_s\mathbf{k}). \tag{3.4}$$

Since the vortex is centered at the origin of (x', y') for any given (z', t'), we can further transform (x', y', z') to a vortex-center-following cylindrical coordinate system (R, β, z'), where

$$R = |\mathbf{x}'| = (x'^2 + y'^2)^{1/2},\ \beta = \tan^{-1}(y', x'), \tag{3.5}$$

and $(x', y') = R(\cos\beta, \sin\beta)$ for given (z', t').

4. 2DVar for axisymmetric-part wind retrieval

a. Control variables and observation operator

The axisymmetric part of the vortex wind, $(\mathbf{u}_s, w_s)$, is assumed to be quasi-stationary in (x', y', z', t') and thus can be expressed as a function of (R, z') to fit to $v_r^{\,i}$ over the analysis time window (≈ 5 min to cover a full volume scan from each radar). In (R, β), $\mathbf{u}_s$ can be conveniently expressed by $\mathbf{u}_s = \mathbf{R}_o V_R + \mathbf{T}_o V_T$, where $\mathbf{R}_o$ (or $\mathbf{T}_o$) is the unit vector along the radial (or tangential) direction, and V_R (or V_T) is the radial (or tangential) component of $\mathbf{u}_s$. For $(\mathbf{u}_s, w_s)$ in (R, z'), the mass continuity equation (3.1) reduces to

$$\partial_R(\rho_o R V_R) + \partial_{z'}(\rho_o R w_s) = 0, \tag{4.1}$$

Constrained by (4.1), the vertical circulation (V_R, w_s) in (R, z') can be expressed by the vertical stream-function ψ_s defined below:

$$\rho_o R(V_R, w_s) \equiv (-\partial_{z'}\psi_s, \partial_R\psi_s). \tag{4.2}$$

The boundary conditions of $w_s = 0$ at $z' = 0$ and $V_R = 0$ at $R = 0$ can be satisfied automatically by setting $\psi_s = 0$ at $z' = 0$ and $R = 0$.

The three components of $\mathbf{u}_s + w_s\mathbf{x}_{cz} + w_s\mathbf{k} \equiv \mathbf{u}^s + w^s\mathbf{k} \equiv (u^s, v^s, w^s)$ can be expressed by the two control variables, ψ_s and V_T, in the following forms:

$$\begin{aligned} u^s &= -\cos\beta\partial_{z'}\psi_s/\rho_o - \sin\beta V_T + x_{cz}w^s, \\ v^s &= -\sin\beta\partial_{z'}\psi_s/\rho_o + \cos\beta V_T + y_{cz}w^s, \\ w^s &= w_s = \partial_R(R\psi_s)/(\rho_o R). \end{aligned} \tag{4.3}$$

The radial component of $\mathbf{u}^s + w^s\mathbf{k}$ in the original (x, y, z, t) space is then given by

$$v_r \equiv \mathbf{r}_o\bullet(\mathbf{u}^s + w^s\mathbf{k}) = (u^s\sin\varphi + v^s\cos\varphi)\cos\theta + w^s\sin\theta, \tag{4.4}$$

where φ is the azimuthal angle (with respect to y-coordinate) of the concerned observation point viewed from the radar site, and θ is as in (3.3). The observation operator that relates the control variables (ψ_s, V_T) to the innovation $v_r^{\,i}$ in (3.3) is thus formulated by (4.3)-(4.4).

b. Cost-function and vortex-flow-dependent background error covariance functions

The cost-function for fitting v_r in (4.3)-(4.4) to $v_r^{\,i}$ in (3.3) is

$$J = \mathbf{a}^T\mathbf{B}^{-1}\mathbf{a}/2 + (\mathbf{Ha} - \mathbf{d})^T\mathbf{O}^{-1}(\mathbf{Ha} - \mathbf{d})/2, \tag{4.5}$$

where $\mathbf{a} \equiv (\mathbf{a}_1^{\,T}, \mathbf{a}_2^{\,T})^T$, $\mathbf{a}_1$ (or $\mathbf{a}_2$) is the state vector of ψ_s (or V_T), $(\,)^T$ denotes the transpose of ( ), $\mathbf{B}$ is the background error covariance matrix, $\mathbf{O}$ is the observation error covariance matrix, $\mathbf{H}$ is the observation operator formulated in (4.3)-(4.4) (for observations from any given radars), and $\mathbf{d}$ is the innovation vector, that is, the state vector of $v_r^{\,i}$ in (3.3). The observation errors are assumed to be uncorrelated, so $\mathbf{O} = \sigma_o^{\,2}\mathbf{I}$, where $\sigma_o^{\,2}$ is the observation error variance and $\mathbf{I}$ is the identity in the observation space.

The background errors of (ψ_s, V_T) are assumed to be uncorrelated and nearly homogeneous in (r, h) with zero mean, where

$$r \equiv [\ln(1 + R/R_c)]/l \ \text{ and } \ h \equiv z'/H. \tag{4.6}$$

Here, the scaling factor for R is set to R_c = 1 km according the averaged horizontal resolution of radar radial-velocity observations, and l = ½ (or H = 1 km) is the de-correlation length (or depth) scale, which is assumed to be the same for ψ_s and V_T and thus is conveniently factored into r (or h).

The above assumed near homogeneity and non-correlation for the background errors of (ψ_s, V_T) imply that the error covariance tensor function has the following diagonal form:

$$\boldsymbol{B} = (B_1, B_2)^{\text{diag}}, \tag{4.7}$$

The two diagonal components of $\boldsymbol{B}$ are modeled by

$$\begin{aligned} B_1 &= \sigma_1^{\,2}C_1(r_i, r_j; h_i, h_j), \\ B_2 &= \sigma_2^{\,2}C_2(r_i, r_j; h_i - h_j), \end{aligned} \tag{4.8}$$

where σ_1 (or σ_2) is the error standard deviation for ψ_s (or V_T), $C_1(r_i, r_j; h_i, h_j)$ and $C_2(r_i, r_j; h_i - h_j)$ are pseudo-correlation functions constructed by

$$C_1(r_i, r_j; h_i, h_j) = C_0(r_i, r_j)C_0(h_i, h_j),$$
$$C_2(r_i, r_j; h_i - h_j) = C_0(r_i, r_j)C_2(h_i - h_j), \quad (4.9)$$

where

$$C_0(r_i, r_j) \equiv \exp[-(r_i - r_j)^2/2] - \exp[-(r_i + r_j)^2/2],$$
$$C_0(h_i, h_j) \equiv \exp[-(h_i - h_j)^2/2] - \exp[-(h_i + h_j)^2/2],$$
$$C_2(h_i - h_j) \equiv \exp[-(h_i - h_j)^2/2].$$

Note that the Gaussian correlation function is modified in $C_0(r_i, r_j)$ by subtracting its mirror image obtained by mirror-reflecting one of the corrected points, either r_i or r_j, with respect to $r = 0$, so $C_0(r_i, r_j)]$ can have the desired property of $C_0(r_i, r_j) = 0$ for $r_i = 0$ or $r_j = 0$ to ensure the analyzed ψ_s and V_T always approach to zero toward the vortex center. The Gaussian correlation function is also modified in $C_0(h_i, h_j)$ by subtracting its mirror image to ensure that the analyzed ψ_s becomes zero at the lower boundary $h = 0$.

The background error covariance matrix **B** in (4.5) is constructed by the covariance functions formulated in (4.7)-(4.9). The square root of **B** can be derived analytically by using the approach developed in section 3c of Xu et al. (2015a), so the cost-function in (4.5) can be preconditioned into the same matrix form as shown in (22) of Xu et al. (2015a). This can greatly improve the computational efficiency. The detailed matrix formulations are lengthy and thus omitted here.

5. 3DVar for asymmetric-part wind retrieval

The asymmetric part of the vortex wind, ($\mathbf{u}_a$, w_a), is also assumed to be quasi-stationary in (x', y', z', t'), so it can be expressed as a function of (R, β, z') to fit to v_r^{is} over the analysis time window ($\approx$ 5 min). In (R, β, z'), $\mathbf{u}_a$ can be expressed by $\mathbf{u}_a = \mathbf{R}_o V_R + \mathbf{T}_o V_T$, where V_R (or V_T) is the radial (or tangential) component of $\mathbf{u}_a$.

In the (x', y', z')-coordinates, $\rho_o \mathbf{u}_a$ can be expressed by

$$\rho_o u_a = -\partial_{y'}\psi + \partial_{x'}\chi \text{ and } \rho_o v_a = \partial_{x'}\psi + \partial_{y'}\chi. \quad (5.1)$$

This implies that $\mathbf{u}_a$ can be partitioned into $\mathbf{u}_a = \mathbf{u}_a^r + \mathbf{u}_a^d$ with $\rho_o \mathbf{u}_a^r \equiv \mathbf{k}\times\nabla'\psi$ and $\rho_o \mathbf{u}_a^d \equiv \nabla'\chi$ for the rotational and divergent parts of $\mathbf{u}_a$, respectively. Thus, V_R and V_T can be partitioned into

$$V_R = V_R^r + V_R^d \text{ with } \rho_o V_R^r \equiv -R^{-1}\partial_\beta\psi \text{ and } \rho_o V_R^d \equiv \partial_R\chi,$$

while V_T can be partitioned into

$$V_T = V_T^r + V_T^d \text{ with } \rho_o V_T^r \equiv \partial_R\psi \text{ and } \rho_o V_T^d \equiv R^{-1}\partial_\beta\chi.$$

The mass continuity equation for the asymmetric part has the form of $\partial_{z'}(\rho_o w_a) = -\nabla'^2\chi$ in (x', y', z') or, equivalently,

$$\partial_{z'}(\rho_o w_a) = -R^{-1}(\partial_R R \partial_R \chi) - R^{-2}\partial_\beta^2\chi \text{ in } (R, \beta, z'). \quad (5.2)$$

By transforming the two control variables, ψ and χ, into

$$X \equiv \int_0^{z'} \chi dz/[\tanh(R/R_o)] \text{ and } Y \equiv \psi/[\tanh(R/R_o)], \quad (5.3)$$

an useful explicit expression of $w_a = -\nabla'^2[X\tanh(R/R_o)]$ is derived from (5.2). Since the analyzed X (or Y) approaches O(R) as $R \to 0$, the transformation introduced in (5.3) can prevent the analyzed divergence $\nabla'^2\chi$ (or vorticity $\nabla'^2\psi$) from becoming singular as $R \to 0$.

The three components of $\mathbf{u}_a + w_a\mathbf{x}_{cz} + w_a\mathbf{k} \equiv \mathbf{u}^a + w^a\mathbf{k} \equiv (u^a, v^a, w^a)$ can be expressed by X and Y in the following forms:

$$u^a = [\cos\beta(F\partial_R\partial_{z'}X + \partial_{z'}X\partial_R F - F\partial_\beta Y/R) - \sin\beta(F\partial_R Y + Y\partial_R F + F\partial_\beta\partial_{z'}X/R)]/\rho_o + x_{cz}w_a,$$
$$v^a = [\sin\beta(F\partial_R\partial_{z'}X + \partial_{z'}X\partial_R F - F\partial_\beta Y/R) + \cos\beta(F\partial_R Y + Y\partial_R F + F\partial_\beta\partial_{z'}X/R)]/\rho_o + y_{cz}w_a,$$
$$w^a = w_a = -[R^{-1}(F\partial_R X + X\partial_R F) + F\partial_R^2 X + 2\partial_R X\partial_R F + X\partial_R^2 F + R^{-2}F\partial_\beta^2 X]/\rho_o. \quad (5.4)$$

The radial component of $\mathbf{u}^a + w^a\mathbf{k}$ in the original (x, y, z, t) space is given by

$$v_r = (u^a\sin\varphi + v^a\cos\varphi)\cos\theta + w^a\sin\theta. \quad (5.5)$$

The observation operator that relates the control variables (X, Y) to the innovation v_r^{is} in (3.4) is thus formulated by (5.4)-(5.5).

The cost-function for fitting v_r in (5.4)-(5.5) to v_r^{is} in (3.4) has the same matrix form as that in (4.5), except that now $\mathbf{a}_1$ (or $\mathbf{a}_2$) is the state vector of X (or Y), **H** is the observation operator formulated in (5.4)-(5.5), **d** is the state vector of v_r^{is}, and **B** is formulated and constructed differently as described below.

The random vector fields of background errors for (X, Y) are assumed to be not correlated and nearly homogeneous with zero mean in (r, β, h), so the error covariance tensor function has the same diagonal form as that in (4.7), but the two diagonal components of $\boldsymbol{B}$ are modeled by

$$B_1 = \sigma_1^2 C_1(r_i, r_j; h_i, h_j; \phi_i - \phi_j),$$
$$B_2 = \sigma_2^2 C_2(r_i, r_j; h_i - h_j; \phi_i - \phi_j), \quad (5.6)$$

where σ_1 (or σ_2) is the error standard deviation for X (or Y), $C_1(r_i, r_j; h_i, h_j; \phi_i - \phi_j)$ and $C_2(r_i, r_j; h_i - h_j; \phi_i - \phi_j)$ are pseudo-correlation functions constructed by

$$C_1(r_i, r_j; h_i, h_j; \phi_i - \phi_j) = C_0(r_i, r_j)C_0(h_i, h_j)C(\phi_i - \phi_j; \boldsymbol{\Phi})$$
$$C_2(r_i, r_j; h_i - h_j; \phi_i - \phi_j) = C_0(r_i, r_j)C_2(h_i - h_j)C(\phi_i - \phi_j; \boldsymbol{\Phi}).$$

Here, $C_0(r_i, r_j)$, $C_0(h_i, h_j)$ and $C_2(h_i - h_j)$ are the same as those used in (4.9), while $C(\phi_i - \phi_j; \boldsymbol{\Phi})$ is similar to that in (16c) of (Xu et al. 2015a) but the de-correlation arc $\boldsymbol{\Phi}$ is no longer constant and is formulated as a function of R to ensure that the de-correlation arc length approaches π in the limit of $R \to 0$ and approaches the de-correlation radial length in R in the limit of $R \to \infty$. (2.6a)

The background error covariance matrix **B** is constructed by the covariance functions formulated in (5.6). The square root of **B** can be derived analytically, again by using the approach developed in section 3c of Xu et al. (2015a), so the cost-function can be preconditioned to improve the

computational efficiency. The detailed matrix formulations are very lengthy and thus omitted here.

6. Results

For the 20 May 2013 Oklahoma Moore mesocyclone, a time series of 3D vortex wind fields are retrieved in 10 consecutive analysis time windows over the same time period (from local time 14:52 to 15:35) as shown in Fig. 1.

The vortex winds retrieved in the second analysis time window (local time 14:55-14:58) are shown in Fig. 2. The retrieval is produced by using one volume radial-velocity scan (on 13 tilts at 0.5°, 0.9°, 1.3°, 1.8°, 2.4°, 3.1°, 4.0°, 5.1°, 6.4°, 8.0°, 10.1°, 12.5°, 15.6°) from the operational KTLX radar and one sector radial-velocity scan (on 10 tilts at 0.5°, 0.9°, 1.3°, 1.8°, 2.4°, 3.0°, 4.0°, 6.4°, 8.0°, 10.0°). The upper panel of Fig. 2 is a vertical cross-section of the axisymmetric part of the vortex flow, and this vertical cross-section is intersected along the slantwise vortex core shown by the vertical profile of $\mathbf{x}_c(z, t)$ plotted by the red line at the local time of t = 14:55 in Fig. 1. As shown by this vertical cross-section, the axisymmetric part of the vortex flow can be characterized distinctly by the following features: (i) a highly slanted vortex core with a ring of maximum tangential velocity in the shallow vertical layer around z = 0.75 km, (ii) a strong downdraft along the slantwise vortex core from the vertical level at z = 2.5 km down to the surface at z = 0, and (iii) a broad updraft tube around the slantwise vortex core above the boundary layer. The lower panel of Fig. 2 shows the horizontal cross-section of the total vortex flow (that is, the sum of the axisymmetric and asymmetric parts) at z = 1 km. This horizontal cross-section reveals the following distinct features for the total vortex flow: (i) a strong cyclonically spiraled downdraft coupled with a weak cyclonically spiraled updraft within and around the vortex core, (ii) a broadly curved updraft around and ahead (to the northeast) of the vortex core, (iii) strong cyclonical rotation with strong divergence for the horizontal flow inside and around the vortex core, and (iv) continuously strong cyclonical rotation but with strong convergence for the horizontal flow to the east ahead of the vortex core.

The vortex winds retrieved in the sixth analysis time window (local time from 15:13 to 15:16) are shown in Fig. 3. The retrieval is produced by using one volume radial-velocity scan (on 11 tilts at 0.5°, 0.9°, 1.4°, 1.8°, 2.4°, 3.1°, 4.0°, 5.1°, 6.4°, 8.0°, 12.5°) from the operational KTLX radar and one sector radial-velocity scan (on 6 tilts at 0.5°, 0.9°, 1.3°, 1.8°, 2.4°, 3.0°). The upper panel of Fig. 3 is a vertical cross-section of the axisymmetric part of the vortex flow, and this vertical cross-section is intersected along the slantwise vortex core shown by the vertical profile of $\mathbf{x}_c(z, t)$ plotted by the red line at the local time of t = 15:13 in Fig. 1. As shown by this vertical cross-section, the axisymmetric part of the vortex flow in this analysis time window can be characterized distinctly by the following features: (i) a nearly vertical vortex core with greatly intensified tangential velocity over the entire depth of the analysis domain (from z = 0 to 5 km), (ii) a lower-level updraft against an upper-level downdraft inside the vortex core, and (iii) a broad updraft tube outside and around the vortex core above the boundary layer. These features are clearly very different from those shown by the vertical cross-section in Fig. 2. The lower panel of Fig. 3 shows the horizontal cross-section of the total vortex flow at z = 1 km. This horizontal cross-section reveals the following distinct features for the total vortex flow at z = 1 km: (i) highly curved areas of strong updraft coupled with weak downdraft within the vortex core, (ii) a broadly curved area of updraft around and ahead of the vortex core. (iii) greatly intensified cyclonical rotation with very strong divergence for the horizontal flow in the area to the east and northeast immediately ahead of the vortex core. The horizontal flow is strongly convergent in the area to the northeast and ahead of the vortex core. In this analysis time window, the retrieved wind speed at the surface level (not shown) exceeds 65 ms^{-1} in the 1 km vicinity southeast of vortex center. By comparing the vortex winds in Fig. 3 with those in Fig. 2, it is easy to see that the vortex winds became increasingly intense as the vortex core became increasingly vertical from the local time 14:55 to 15:16.

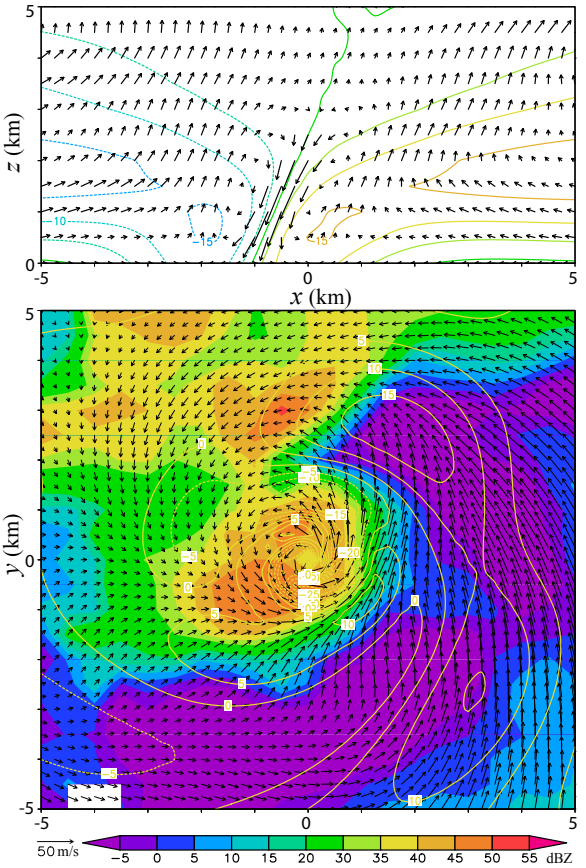

Fig. 2. Vortex winds retrieved in the second analysis time windows (from local time 14:55 to 14:58) from radial-velocity observations collected by the operational KTLX radar and the NSSL phased-array radar. The upper panel shows the vertical cross-section (along the slantwise vortex core shown by the red line at local time 14:55 in Fig. 1) of the axisymmetric part of vortex winds with the vertical circulation plotted by arrows and the tangential velocity plotted by contours of every 5 ms^{-1}. The lower panel shows the horizontal cross-section at z = 1 km for the total vortex winds with the horizontal velocity field plotted by arrows and the vertical velocity field plotted by contours of every 5 ms^{-1} superimposed on the colored reflectivity field. The color scale for reflectivity is shown at the bottom of the figure.

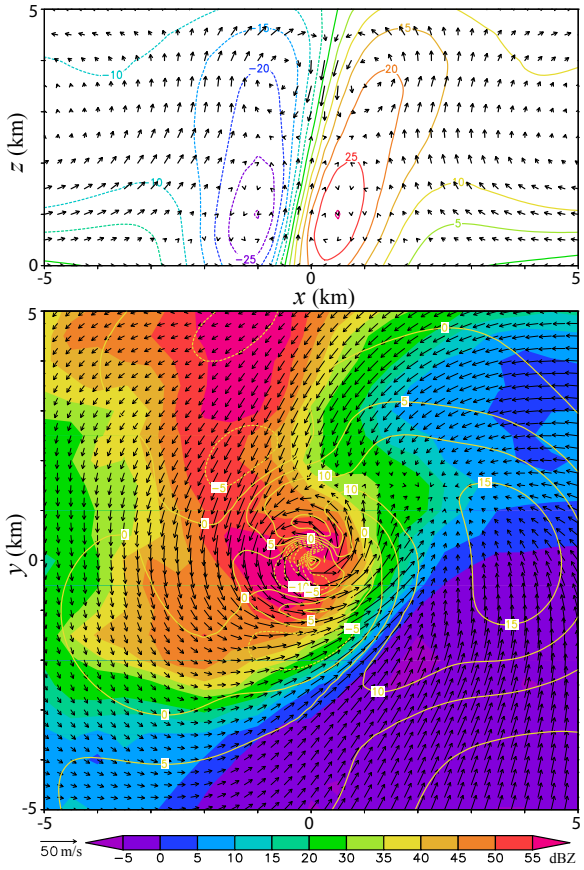

Fig. 3. As in Fig. 2, but for vortex winds retrieved in the sixth analysis time window (from local time 15:13 to 15:16).

7. Conclusions

As an extension of the 2DVar method for retrieving tornadic mesocyclone winds from radar observations (Xu et al. 2015a), a 3DVar method is developed in this paper to retrieve 3D vortex winds of tornadic mesocyclones from radar observations in the 4D space. This method has the following features: (i) The vortex center is estimated as a continuous function of (z, t) in the 4D space from radar observations. (ii) The retrieval domain is co-centered and moving with the slantwise vortex core at each vertical level. (iii) Vortex-flow-dependent background error covariance functions are formulated with the mass continuity equation and boundary conditions satisfied automatically.

The method has been successfully applied to radial-velocity observations from the operational KTLX and the NSSL phased-array radar for the tornadic mesocyclone that struck Moore in Oklahoma on 20 May 2013. The retrieved vortex wind fields reveal that the mesocyclone vortex core became increasingly vertical and the vortex became increasingly intense as the mesocyclones moved toward Moore. Like the 2DVar method, as shown in Xu et al. (2015a), the 3DVar method can be also incorporated into the radar wind analysis system (Xu et al. 2015c) as an additional step of targeted fine-scale analysis to produce high-resolution 3D wind fields for storm-scale data assimilation. This capability is currently being developed.

Acknowledgments

The research work was supported by the Warn-on-Forecast project at NSSL and the ONR Grant N000141410281 to the University of Oklahoma (OU). Funding was also provided to CIMMS by NOAA/Office of Oceanic and Atmospheric Research under NOAA-OU Cooperative Agreement #NA17RJ1227, U.S. Department of Commerce.

REFERENCES

Gao, J., T. M. Smith, D. J. Stensrud, C. Fu, K. Calhoun, K. L. Mnaross, J. Brogden, V. Lakshmanan, Y. Wang, K. W. Thomas, K. Brewster, and M. Xue, 2013: A realtime weather-adaptive 3DVAR analysis system for severe weather detections and warnings. *Wea. Forecasting*, **28**, 727–745.

Xu, Q., K. Nai, S. Liu, C. Karstens, T. Smith and Q. Zhao, 2013: Improved Doppler velocity dealiasing for radar data assimilation and storm-scale vortex detection. *Advances in Meteorology*. vol. **2013**, Article ID 562386, 10 pages.

Xu, Q., L. Wei and K. Nai, 2015a: Analyzing vortex winds in radar observed tornadic mesocyclones for nowcast applications. *Wea. and Forecasting*, **30**, 1140–1157.

Xu, Q., L. Wei and K. Nai, 2015b: Estimating vortex center locations and movements in four-dimensional space from radar observed tornadic mesocyclones. *37th Conference on Radar Meteorology*, 14-18 September 2015, Norman, OK, Amer. Meteor. Soc., 14A.2.

Xu, Q., L. Wei, K. Nai, S. Liu, R. M. Rabin, and Q. Zhao, 2015c: A radar wind analysis system for nowcast applications. *Advances in Meteorology*. vol. **2015**, Article ID 264515, 13 pages.

Xu, Q. and L. Wei, 2013: Prognostic equation for radar radial velocity derived by considering atmospheric refraction and earth curvature. *J. Atmos. Sci.*, **70**, 3328–3338.